JOURNAL OF CATALYSIS 136, 554–565 (1992)

Heterogeneous Photocatalytic Oxidation of Gas-Phase Organics for Air Purification: Acetone, 1-Butanol, Butyraldehyde, Formaldehyde, and *m*-Xylene Oxidation

JOSÉ PERAL AND DAVID F. OLLIS

Department of Chemical Engineering, North Carolina State University, Raleigh, North Carolina 27695-7905

Received December 20, 1991; revised February 20, 1992

Photocatalyzed degradations of trace levels of various oxygenates and an aromatic in air were carried out using near-UV-illuminated titanium dioxide (anatase) powder. The initial rates of degradation for acetone, 1-butanol, formaldehyde, and *m*-xylene were well described by Langmuir–Hinshelwood rate forms. No reaction intermediates were detected for acetone oxidation at conversions of 5–20%. Butyraldehyde was the main product of 1-butanol oxidation for conversions of 20–30%. The influence of 5% water (simulating partial humidification) in the feedstream varied strongly: water vapor inhibited acetone oxidation, but had no influence on the 1-butanol conversion rate. *m*-Xylene conversion was enhanced by trace water addition, but inhibited at higher water levels. Some catalyst deactivation was detected between 1-butanol runs; the activity could be easily recovered by illuminating the catalyst in fresh air. Formaldehyde was also successfully oxidized. These results, taken together with earlier literature citations for photocatalyzed total oxidation of methane, ethane, trichloroethylene (but see (*27*)), toluene, and a very recent report for oxidation of odor compounds, indicate a favorable technical potential for photocatalyzed treatment of air in order to degrade and remove all major classes of oxidizable air contaminants.

INTRODUCTION

The removal of undesired organic contaminants in air has been a topic of major and continuing emphasis over the last decade. Potential application sites for air purification and decontamination technologies include completely or partially enclosed atmospheres such as those found in spacecraft, office buildings, factories, and homes. As a large number of the common air contaminants of concern are oxidizable, the need for an oxidative destruction process is self-evident. Heterogeneous catalytic oxidation technology for gas-phase pollution control has well-established examples in automotive exhaust and catalytic incineration. However, nearly all heterogeneous oxidation catalysts function at elevated temperatures, whereas nearly all inhabited atmospheres of concern to humans exist at or near 20–25°C. Further, a need exists for an air purification catalyst which can not only function at ambient conditions of temperature and pressure, but can also use the mildest and most prevalent oxidant, molecular oxygen (O_2), and is active against the broadest possible range of contaminant structures.

One oxidation catalyst candidate that operates at room temperature using molecular oxygen is a photocatalyst. Heterogeneous photocatalysis is the ambient temperature process in which the surface of an illuminated semiconductor acts as a chemical reaction catalyst by using bandgap light as a source of solid excitation. These semiconductor compounds usually have a moderate energy bandgap (1–3.7 eV) between their valence and conduction bands. Under illumination with photons of bandgap or greater energy, the valence band electrons are photoexcited into the conduction band, creating highly reactive electron-hole pairs, which,

0021-9517/92 $5.00

after migrating to the solid surface, may participate in charge-transfer reactions with adsorbates and provoke the reduction or oxidation of such species.

Most of the heterogeneous photocatalysis reports of the last decade have dealt with aqueous solutions, exploring water decontamination and purification by the photoassisted oxidative destruction of hazardous solutes (*1–3*).

Studies involving gas-phase heterogeneous photocatalysis are far fewer, but the modest existing literature has demonstrated that near-UV illumination in concert with anatase titanium dioxide (TiO_2) photocatalyst and molecular oxygen can carry out the complete oxidation of several small hydrocarbons (methane and ethane) (*4*), an aromatic (toluene) (*5*), a halocarbon [trichloroethylene (TCE)] (*6*) (but see (*27*)), and carbon monoxide (*4*). The heterogeneous photooxidations of some of the organics examined out in the present paper have been previously reported by other authors using much higher reactant concentrations: Blake and Griffin (*7*) studied 1-butanol heterogeneous photooxidation for 1 : 21 molar ratios of butanol : oxygen and Stone *et al.* (*8*) reported photooxidized acetone at 10% concentration in an O_2 atmosphere. Finally, in a very recent paper, Suzuki *et al.* (*9*) reported use of immobilized TiO_2 for photocatalytic air deodorization. Their brief (two-page) paper presented evidence for photocatalyzed oxidation of acetaldehyde, isobutyric acid, toluene, methylmercaptan, hydrogen sulfide, and trimethylamine. They reported only a single run for each reactant (with initial concentrations between 5 and 80 ppm) and suggested that the variation of reactant with time was first order.

The present gas–solid photocatalysis study was undertaken for two reasons:

(i) A survey of the literature on spacecraft, office, building, and factory air quality indicates that a central class of offending chemicals are oxygenates, e.g., aldehydes, ketones, and alcohols. Accordingly, we initiated and report here an examination of the photocatalytic destruction of formaldehyde, butyraldehyde, acetone, and 1-butanol.

(ii) With the exception of the toluene (*5*), TCE (*6*), and Suzuki (*9*) reports, all prior studies were for organic vapor-phase concentrations much higher than the 1–500 ppm (mass) characteristic of short-term exposure standards or odor threshold levels. Accordingly we wished to explore conversion kinetics at the very low contaminant pressures appropriate to lightly contaminated air at 1 atm.

As application to air treatment in habitable atmospheres is our focus, we also examined the importance of relative humidity on observed rates, as Ibusuki *et al.* (*5*) and Dibble and Raupp (*6*) have each noted a strong but contrasting rate influence of water concentration in the range of conventional air humidification.

EXPERIMENTAL

Figure 1 shows a schematic of the flow reactor experimental system used for the photooxidation studies. UHP air tank (Linde) was used to bring a 20.11 liter gas reservoir to 1 atm. A suitable amount of contaminant in liquid form was then injected into the reservoir through a sample port. Following complete vaporization, the reservoir was filled with additional air up to a final pressure (typically 2.18×10^5 N/m^2), which was sufficient to provide the desired gas-flow rates over periods up to several hours. An air stream from the tank and a gas mixture stream from this lightly pressurized reservoir were mixed continuously and passed to the reactor through mass-flow sensor controllers coupled to a mass-flow controller unit (Linde FM4574). A broad range of contaminant feed concentrations could be examined for flow reactor studies by variation of the two stream rates relative to each other.

The photoreactor was a cylindrical vessel (4 cm high and 3.14 cm^2 base) with an interior, attached fritted glass plate used to support the powdered photocatalyst, through

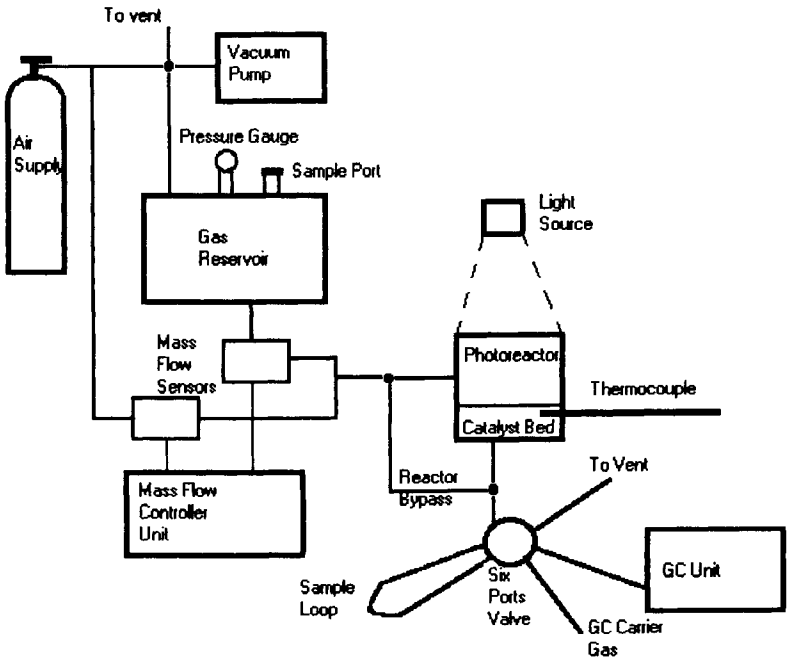

FIG. 1. Experimental system.

which the downward flow passed. An airtight quartz window enclosed the reactor top. Two lateral ports provided the inlet and outlet for the gas mixture, and a thermocouple (always in the dark) was installed just downstream of the glass frit. The photoexcitation light source was placed directly above the reactor window.

A gas sampling loop allowed capture of aliquots of either the reactant feed or the product stream. Except with formaldehyde feeds, all vapor samples were analyzed by gas chromatography (Perkin–Elmer Sigma 1) operating with a flame ionization detector (FID). An SS Alltech column with AT-1000 (1%) on 60/80 Graphac GB packaging was used for acetone, 1-butanol, and butyraldehyde analysis. For *m*-xylene, an SS Alltech with AP-L 15% on 80/100 Chrom W packing was preferred. Formaldehyde analysis was performed by first passing the reactor product gas stream through adsorption tubes containing *N*-benzylethanolamine (Supelco ORBO 22 tubes); this chemical reacted with formaldehyde to form 3-benzyloxazolidine (*10*), which in turn could be analyzed by capillary gas chromatography. For GC–MS identification analysis, samples were first concentrated by passing the reactor exhaust through charcoal tubes and subsequently extracting and diluting the adsorbate content in a suitable organic solvent. A Hewlett–Packard 5985B was used for these measurements.

The catalyst used was P25 TiO_2 (Degussa) with a primary particle diameter of 30 nm, a surface area of 50 ± 15 m^2/g, and a crystal structure of primarily anatase. The P25 particles were spherical and nonporous, with a stated purity of >99.5% TiO_2. Stated impurities included: Al_2O_3 (<0.3%), HCl (<0.3%), SiO_2 (<0.2%), and Fe_2O_3 (<0.01%). This powdered semiconductor catalyst was used as supplied without pretreatment. The acetone, 1-butanol, and butyraldehyde used to prepare individual gas mixtures were of HPLC grade, supplied by Aldrich. The formaldehyde source was a 37% (W/W) aqueous solution containing 10–15% methanol as a stabilizer.

Either of two light sources was used: a 200-W high-pressure Hg–Xe lamp (Oriel Corp.) or a 100-W blacklight (UVP). To prevent any true UV (200–300 nm) homogeneous photoreaction, a Pyrex plate was positioned over the reactor window to absorb the incident radiation having $\lambda < 300$ nm and to transmit only the near-UV light for the TiO_2 photoactivation. Neutral screens were used for the intensity variation studies, and the resultant incident light fluxes were measured with ferrioxalate liquid actinometers placed under the quartz-reactor window.

In a typical experiment, 0.1 g of TiO_2 powder was spread uniformly over the surface of the porous fritted glass plate, providing a 3.2-mm TiO_2 powder layer. Both the catalyst and the fritted glass had appreciable surface areas. For the previous photocatalyst partial oxidation studies, which involved reactant partial pressures of 0.1 to several atmospheres, these surfaces would have come rapidly to a gas–solid equilibrium in a flow reactor. With our only slightly contaminated air feed, however, the surface inventory of strongly held reactant required some time to accumulate to a "dark" gas–solid equilibrium. Consequently, the trace contaminated air had first to be fed for a considerable period of time (typically 60–90 min) until the feed and reactor exit gas concentrations were identical (no dark reaction products were noted). When that condition was achieved, the light was turned on, and gas samples were taken every 10–20 min. The irradiation was maintained for a convenient period of time (2–6 h) to establish that the photo-steady-state was achieved. Gas-flow rates of 70–120 ml/min were used through all experiments, providing reaction rates that were essentially free of mass transfer influences, as shown by calculation of the mass transfer coefficient in packed-bed reactors (*11*) (see Appendix).

RESULTS

Acetone Photooxidation

Our experiments used very low acetone gas-phase concentrations (75–250 mg/m^3). Dark acetone gas mixture flows over the TiO_2 showed a moderate equilibrated extent of acetone adsorption (0.206 mg acetone/100 mg TiO_2), corresponding to an initial surface coverage of 0.85 acetone molecules/nm^2.

Under illumination, a substantial decrease of the acetone exit concentration was noted, and no oxidizable products of reaction were found by FID. Formaldehyde, if formed, has a very small heat of combustion which would have prevented its FID detection. Conversions of 15–20% were achieved under the reported experimental conditions.

As the activity of the illuminated catalyst was sufficient to provide appreciable conversion of acetone, we consider a simple plug-flow integral analysis of the data in order to describe the change of acetone concentration through the illuminated outermost TiO_2 layer, where light absorption takes place. The reaction rate constant will vary with intensity I as I^α with $\alpha = 1$ at very low intensities (*12, 13*) and $\alpha = 0.5$ at very high values (*12, 14*). Over the single decade variation in irradiance used here, the reaction rate constant will depend on the intensity of light at any depth and on the value of the exponent α (taken to be constant):

$$k = k_0 \left(\frac{I}{I_0}\right)^\alpha = k_0 e^{-\alpha \varepsilon z}, \qquad (1)$$

where ε is the effective adsorption coefficient of TiO_2 and z the axial coordinate through the TiO_2 layer.

Langmuir–Hinshelwood (LH) rate forms have been widely used in liquid-phase photocatalysis and have been found of utility in gas-phase TCE destruction (*6*) and alkane partial oxidation (*15*). Assuming an LH form for the present systems, plug flow through our thin packed bed gives

$$\nu \frac{dC}{dz} = -\frac{kKC}{1 + KC} = -\frac{k_0 e^{-\alpha \varepsilon z} KC}{1 + KC}, \qquad (2)$$

where ν is the gas linear velocity and C is the gas-phase concentration of acetone. Integration of Eq. (2), assuming complete light absorption, and rearrangement gives

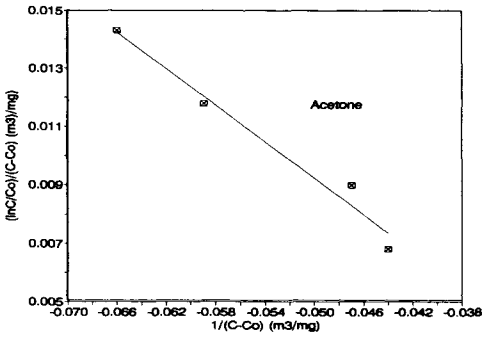

FIG. 2. Plot of $(C - C_0)^{-1} \cdot \ln(C/C^0)$ vs $(C - C_0)^{-1}$ for acetone data in Table 1. $I_a = 3.5 \times 10^{-7}$ Einstein/cm_2 · min (200-W high-pressure Hg–Xe lamp); T = 22–24°C.

$$\frac{\ln(C/C_0)}{C - C_0} = -\frac{k_0 K}{\alpha \varepsilon \nu} \frac{1}{C - C_0} - K. \quad (3)$$

If the assumed LH form is valid, then a plot of $(C - C_0)^{-1} \cdot \ln(C/C°)$ vs $(C - C_0)^{-1}$ should be linear; Fig. 2 indicates that the experimental data are in good agreement with this integral rate-law analysis. Values of k and K can be calculated if the TiO_2 absorption coefficient ε and the exponent α are previously known. As reported by Courbon *et al.* (*4*), 99% of light absorption (optical density 2) occurs within a TiO_2 anatase layer of 4.5 μm, and so an ε value of 10211 cm^{-1} was estimated. Values of k = 7.75 g/liter · min and K = 0.00644 m^3/mg were then calculated from the intercept and slope in Fig. 2, when α = 0.7 as found below.

The photocatalyzed oxidation rate was expected to be intensity dependent, as reflected in prior literature. A plot of log acetone rate vs log I_a (incident irradiation) gives a straight line of slope 0.7 ± 0.1 (Fig. 3). Thus the reaction rate follow.

$$\text{Rate} = K' I_a^{0.7} f(\text{reactant}). \quad (4)$$

This equation describes a transition regime (α = 0.7) between the two asymptotic values reported above ($0.5 \leq \alpha \leq 1.0$).

The photocatalytic efficiency of utilization of light to drive the desired oxidation reaction is represented by the apparent quantum yield, q, defined by q = molecules reacted/photons absorbed. This calculated apparent quantum yield is plotted vs irradiance in Fig. 3. For the present acetone oxidation, q varies as

$$q \propto \frac{\text{rate}}{I'_a} \propto \frac{I_a^{0.7}}{I'_a} = I_a^{-0.3}. \quad (5)$$

Water in the gas feed inhibits the acetone oxidation rate. The dependence of rate on the water concentration may be described by the relationship

$$r = \frac{r_0}{1 + K_H[H_2O]^\beta}, \quad (6)$$

where r_0 is the reaction rate free of water effect. Figure 4 shows that experimental data can be fitted by the equation $1/r = 1100 + 0.00106[H_2O]^{1.674}$, which is the inverse of Eq. (6):

$$\frac{1}{r} = \frac{1}{r_0} + \frac{K_H}{r_0}[H_2O]^\beta. \quad (7)$$

From this data fitting we obtain $\beta \approx 1.7$, r_0 = 0.909 μg/min · cm^2, and $K_H = 9.6 \times 10^{-7}$ m^3/mg.

1-Butanol Photooxidation

For fresh catalyst in the dark, considerable time (2 h) was required to achieve a reactor exit concentration equal to the feed

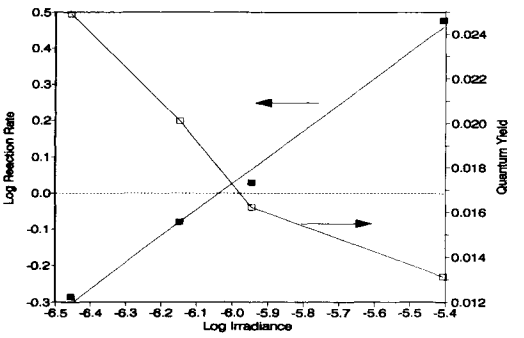

FIG. 3. Reaction rate of acetone photooxidation and quantum yield vs irradiance. $[Acetone]_0$ = 160 mg/m^3; T = 22–24°C. Reaction rate and irradiance units are $\mu g/cm^2$ · min and Einstein/cm^2 · min, respectively.

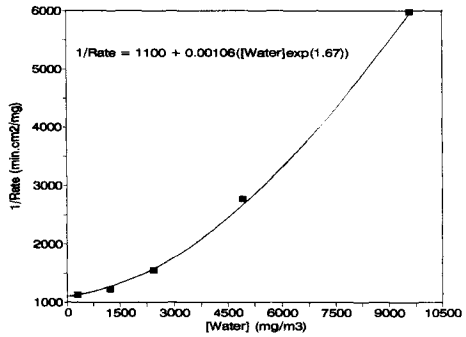

FIG. 4. Inverse of reaction rate of acetone photooxidation vs water concentration in the gas phase. $[\text{Acetone}]_0$ = 200 mg/m^3; T = 22–24°C. 200-W high-pressure Hg–Xe lamp. Reaction rate and water concentration units are mg/cm^2 · min and mg/m^3, respectively.

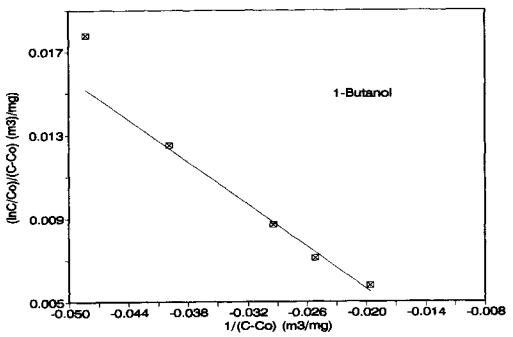

FIG. 5. Plot of $(C - C_0)^{-1} \cdot \ln(C/C^0)$ vs $(C - C_0)^{-1}$ for 1-butanol data in Table 1. $I_a = 5.0 \times 10^{-7}$ Einstein/cm^2 · min (100-W blacklight); T = 22–24°C.

value. The integrated Δ concentration difference of flow over time indicated that 2.01 mg of 1-butanol was adsorbed onto the catalyst (100 mg) and frit. This value indicates 10 times more mass adsorption for 1-butanol than for acetone and corresponds to a surface coverage of 5.88 1-butanol molecules/nm^2 TiO_2. These results confirm a strong affinity between the alcohol and the metal oxide surface.

Under illumination, the 1-butanol steady-state exit concentration was decreased and two intermediate products peaks appeared (major and minor). The largest of the two new peaks observed in the present study was verified as butyraldehyde by direct injection of this organic for its GC–FID detection. Attempts to associate the trace, second GC peak with butene by direct injection of 1-butene were unsuccessful.

Butyraldehyde heterogeneous photooxidation experiments were also carried out with a mixture of 118 mg/m^3 of this reactant. A steady-state reaction rate of 1.5 μg/cm^2 · min was achieved after 150 min. A secondary GC peak was observed, with retention time identical to that of the unknown detected during 1-butanol photooxidation. That peak may thus correspond to a product of butyraldehyde oxidation rather than the suspected 1-butene formed through dehydration of 1-butanol.

The rates calculated from 1-butanol data can be fitted by using the integral LH rate form developed above (Fig. 5). The apparent rate and binding constants of 1-butanol are k = 49.2 g/liter · min and K = 0.00109 m^3/mg, respectively.

Variations in water vapor content have no significant effect on the rate of disappearance of 1-butanol or the rate of butyraldehyde formation (Fig. 6).

Photocatalyst Deactivation

In 1-butanol photooxidation experiments, steady states achieved after successive dark periods indicated a transient catalyst deacti-

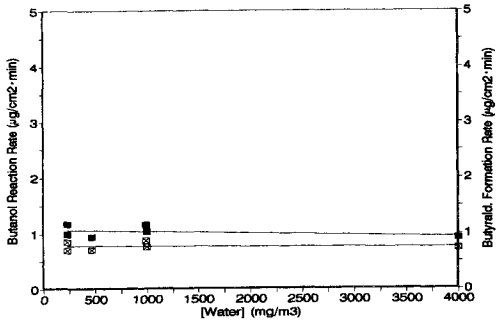

FIG. 6. Reaction rate of 1-butanol photooxidation and butyraldehyde formation vs water concentration in the gas phase. $I_a = 5.0 \times 10^{-7}$ Einstein/cm^2 · min (100-W blacklight); T = 22–24°C.

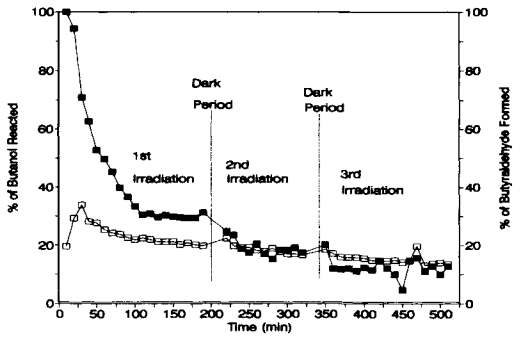

FIG. 7. Deactivation of photo-steady-state for 1-butanol conversions (see text for details). $[Butanol]_0$ = 260 mg/m^3; $I_a = 5.0 \times 10^{-7}$ Einstein/cm^2 · min; T = 22–24°C.

vation taking place just after each dark period (Fig. 7). The butyraldehyde formation rate also decreased after dark and reillumination periods. At these eventual steady states, the 1-butanol consumed equalled the butyraldehyde produced, and the concentration of the unknown second product was virtually zero. This behaviour was found in a range of 1-butanol concentrations of 140–260 mg/m^3.

Verification that steady-state conditions were achieved was accomplished through "long-term" illuminations of more than 6 h, carried out in the presence of 1000 mg/m^3 water in the gas feed. When similar experiments were repeated in the total absence of water in the feed, catalyst activity loss was continuous and no steady-state conditions were achieved. This latter continuous loss of activity is in agreement with the essential need of surface water for the occurrence of photoassisted oxidation over metal oxides as reported by others (*6, 16*).

To regenerate catalyst activity following deactivation in 1-butanol experiments, different catalyst treatments were explored. Only replacement of contaminated air by pure air (with no water vapor) and continued overnight illumination and flow resulted in a progressive regeneration of most catalyst activity. This result indicates that some strongly adsorbed, oxidizable intermediate or side products must be responsible for the photoactivity decay; the intermediate can in turn be photooxidized but at lower rates than 1-butanol oxidation.

Operations at above ambient temperatures (61–62°C or 75–80°C) were examined. No noticeable rate differences were found with reaction temperature, and after each new dark period, deactivation again occurred to give lower steady-state 1-butanol conversions, with nearly exclusive butyraldehyde formation.

The same transient decay of photocatalytic activity after dark periods was observed when photooxidizing butyraldehyde; the species responsible for the deactivation may be the same in both cases.

Formaldehyde Photooxidation

Formaldehyde has been reported (*8*) to be a trace intermediate of acetone photooxidation, and it might be expected to occur as an intermediate in the final steps of other organic oxidations. In our preliminary experiments, high conversions (55–85%) of formaldehyde were obtained, and the destruction of this pollutant down to levels of 1 ppm, which corresponds to its threshold limit value-time-weighted average (*17*), appears to be possible by heterogeneous photocatalysis. Figure 8 shows that our limited formaldehyde data also fit the integrated LH rate law; the deviant point corresponds to

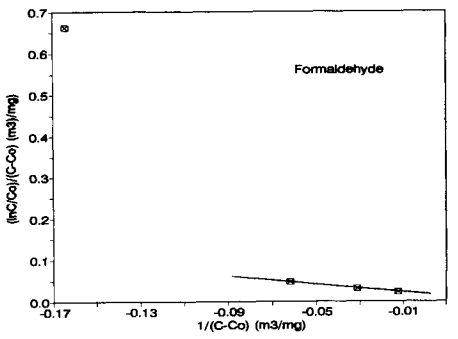

FIG. 8. Plot of $(C - C_0)^{-1} \cdot \ln(C/C^0)$ vs $(C - C_0)^{-1}$ for formaldehyde data in Table 1. $I_a = 5.0 \times 10^{-7}$ Einstein/cm^2 · min (100-W blacklight); T = 22–24°C.

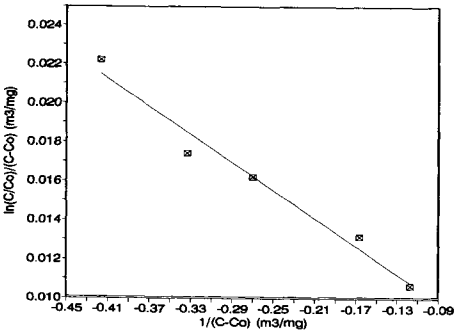

FIG. 9. Plot of $(C - C_0)^{-1} \cdot \ln(C/C^0)$ vs $(C - C_0)^{-1}$ for *m*-xylene data in Table 1. $I_a = 5.0 \times 10^{-7}$ Einstein/cm^2 · min (100-W blacklight); T = 22–24°C.

an estimated outlet concentration of 0.1 ppm formaldehyde, which is well below our analytical limitations of about 1 ppm; we are currently exploring improvements in our detection limits. Simultaneous photocatalytic oxidation of methanol, present as a formaldehyde solution stabilizer, was confirmed by means of direct GC–FID analysis.

m-Xylene Photooxidation

As an example of trace level gas-phase photooxidation of aromatic compounds, we include here data of *m*-xylene oxidation. Ibusuki and Takeuchi (*5*) have reported the TiO_2-assisted photooxidation of toluene in air and found that 80 ppm of this reactant could be completely oxidized to CO_2, with formation of less than 1 ppm of benzaldehyde as the only detectable intermediate at a toluene conversion of approximately 80%. The amount of CO_2 formed for a 10-min reaction time was found to increase linearly with percentage relative humidity.

For steady-state *m*-xylene heterogeneous photooxidation, the integrated LH rate form again describes reactant disappearance (Fig. 9), with K = 0.00659 m^3/mg and k = 1.30 g/liter · min. No reaction intermediates were detected by GC–FID. In the hypothetical case of formation of an aldehyde derivative at 1% of total reactant, like the benzaldehyde found by Ibusuki and Takeuchi, this low amount would probably not have been detected.

Water vapor influences *m*-xylene photooxidation reaction rate appreciably (Fig. 10); the rate increases with the water content up to values of 1000–1500 mg/m^3 and decreases thereafter, as indicated by the approximately inverse variation of rate with water vapor content above 3000 mg/m^3.

DISCUSSION

Under illumination of wavelengths <370 nm, the valence band electrons of the TiO_2 can be excited to the conduction band, creating highly reactive electron-hole pairs, which, after migration to the solid surface, can be trapped at different sites. The nature of these sites and the trapping mechanisms are yet a subject of discussion among researchers, but it seems quite well accepted that the final electron traps for vapor–solid photocatalysis are the oxygen species on the surface, with O_2^- or O^- being the products of that electron transfer, as indicated for example by the dependence of photoconductance on P_{O_2} (*18*). Munuera *et al.* (*19*) suggested that Ti^{4+} centers capture the conduction band electrons and the Ti^{3+} ions formed are responsible for oxygen photoadsorption. At the same time the photogenerated holes are trapped by hydroxyl ions or water on the surface, producing hydroxyl radicals. The following mechanism represents these initial reaction steps:

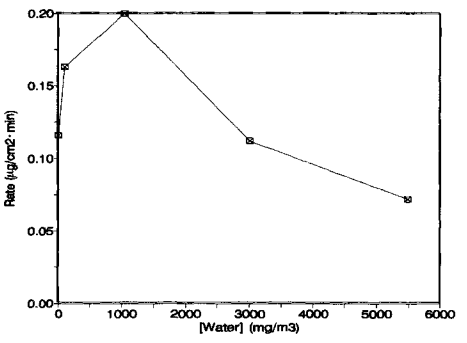

FIG. 10. Reaction rate of *m*-xylene photooxidation vs water concentration in the gas phase. $I_a = 5.0 \times 10^{-7}$ Einstein/cm^2 · min (100-W blacklight); T = 22–24°C.

$$TiO_2 + h\nu \rightleftharpoons h^+ + e^-$$

$$h^+ + OH^- \rightarrow OH\cdot$$

$$Ti^{4+} + e^- \rightarrow Ti^{3+}$$

and

$$Ti^{3+} + O_{2ads} \rightarrow Ti^{4+} + O^-_{2\,ads}$$

or

$$O_{2ads} \rightarrow 2O_{ads}$$

$$Ti^{3+} + O_{ads} \rightarrow Ti^{4+} + O^-_{ads}$$

This mechanism of charge trapping is supported by the observation that oxygen photoadsorption is increased with increased surface hydroxyl concentration and does not take place on completely dry surfaces (*20*). The hole trapping by the hydroxyl species prevents electron-hole recombination at the surface, thus allowing oxygen chemisorption and electron transfer. Two types of hydroxyls, differing by the strength of the bond formed with the surface, have been found by IR studies (*21, 22*), isotopic exchange, and adsorption–desorption measurements (*20*). The less strongly bound hydroxyls are easily removed at modest temperatures, and this occurence does not affect the photocatalytic activity. In contrast, removal of the strongly bound hydroxyls results in complete activity loss (*20*). For these reasons, the hydroxyl radical derived from water is widely accepted as a primary oxidant in heterogeneous photocatalysis; in vapor–solid photocatalysis, direct hole oxidation of adsorbed reactant is also a possibility.

The mechanism of the hydroxyl radical attack depends on the type of organic involved. For example, alcohol oxidation over metal oxide surfaces may take place through two different reaction pathways: the formation of an aldehyde (dehydrogenation reaction) or an olefin (dehydration reaction), each with the same number of carbons (*23*). Blake and Griffin (*7*) found both butyraldehyde and 1-butene to be formed during the photocatalyzed oxidation of 1-butanol over TiO_2 at butanol/oxygen ratios much higher (1 mol butanol/22 mol O_2) than those used in our study. They concluded that these products are formed by parallel reactions from the same intermediate. A suggested mechanism involved hydroxyl radical attack of adsorbed alcohol to give aldehyde and water, both subsequently desorbing, or a dehydration leading to desorption of water and olefin. Under our steady-state conditions, the hydroxyl–alcohol reaction is completely dominant, and only a trace second product is observed.

In acetone photooxidation, we detected no reaction intermediate; prior studies by Bickley *et al.* (*8*) on rutile TiO_2 at much higher partial pressures have reported trace H_2CO formation with CO_2 and water as the major and final products. Djeghri and Teichner (*24*) found acetone to be the only major intermediate of the photocatalytic oxidation of isobutane under hydrocarbon-rich conditions. No subsequent organic intermediates were reported, and these authors showed that acetone and other organics yielded CO_2 as the final photooxidation products over TiO_2 (*25*). Thus, our trace concentrations of acetone studied appear to be cleanly converted to CO_2 and water by means of heterogeneous photocatalysis over TiO_2.

The apparent high reactivity of formaldehyde (and methanol) which we observed is consistent with the finding by Suzuki *et al.* (*9*) that photocatalyzed oxidation of another small oxygenate, acetaldehyde, proceeds so rapidly through any intermediates that none were detected and the molar ratio of CO_2 produced per acetaldehyde consumed was 2 at all conversions studied.

Widely differing rate influences of water have been reported for different photocatalyzed vapor-phase oxidations. Several authors have previously reported the need for traces of water (hydroxyl groups) on the TiO_2 surface in order to maintain vapor-phase photocatalytic oxidation activity for extended periods of time (*6, 20*). Dibble and Raupp (*6*) found the rate of trichloro-

ethylene oxidation to be zero order in water for H_2O mole fractions below 10^{-3} and to become strongly inhibitory with a -3-order rate dependence for water mole fractions between 5×10^{-3} and 5×10^{-2}. In contrast, Ibusuki and Takeuchi (*5*) found that the photocatalyzed oxidation rate of trace toluene (80 ppm) in air was enhanced by water vapor, increasing almost linearly with water vapor content between 0 and 60% relative humidity. In the present study, water vapor feed concentrations of 250 to 10000 mg/m^3 (0.6 to 25% of relative humidity) are clearly inhibitory for acetone photooxidation, but do not affect the rate of 1-butanol reaction. *m*-Xylene oxidation increases with increasing water vapor concentration up to 1000 mg H_2O/m^3 and decreases thereafter.

These behaviors may be explained in terms of adsorption competition: acetone appears to be less strongly adsorbed onto the TiO_2 than 1-butanol; thus water may displace surface-adsorbed acetone but not 1-butanol, and thereby inhibit photocatalyzed oxidation of the former but not the latter. The variable role of water in *m*-xylene photooxidation may follow that of TCE (*6*), where trace water was required for activity, but excess water was inhibitory. The strong adsorption of 1-butanol would explain also the detection of butyraldehyde as a desorbed intermediate.

Photocatalyst deactivation during alcohol oxidation has been reported previously by Cumningham and Hodnett (*26*), who examined 2-butanol and 2-propanol over illuminated TiO_2 and ZnO at concentrations (about 25000 ppm) of alcohol much higher than those of our study. Deactivation profiles seen were similar to ours found at 160–260 mg/m^3 (about 120–200 ppm). The authors suggested that CO_2 product bound to the surface could block some reactive sites, leading to surface deactivation. Rate data with CO_2 added over ZnO that were consistent with this hypothesis were presented, but no data or reference to TiO_2 was offered.

Since all oxidations produce CO_2 but deactivation has only been noted for alcohols, a more likely explanation of this deactivation peculiar to alcohols is that some other reaction product is able to deactivate or block some sites. This adsorbed material is oxidizable under appropriate conditions, since our catalyst may be regenerated photocatalytically in pure air as noted. Also, the achievement of steady-state conditions within every illumination period indicates that the deactivation agent eventually disappears at the same rate as its formation.

The amounts of intermediate products that remain adsorbed onto the catalyst after illumination could be responsible for the deactivation reported after every dark period. If one intermediate was sufficiently reactive, the deactivating species could be formed under dark conditions. Blake and Griffin (*7*) proposed an interesting mechanism of photooxidation for 1-butanol, which involved not only butyraldehyde and butene formation as discussed above but also the formation of butanoic acid from butyraldehyde, in order to rationalize the slow appearance of carboxylate IR bands. Because butanoic acid is expected to be strongly adsorbed onto the TiO_2 surface and because any adsorbed aldehyde may be quite reactive, the acid may be responsible for our slow catalyst deactivation, which is enhanced during each dark period by the dark oxidation of the remaining butyraldehyde. The regeneration could then be due to photocatalyzed decarboxylation, by direct hole attack on adsorbed carboxylate to give

$$R\mathrm{COO}^-(\mathrm{ads}) + h^+ \rightarrow R\mathrm{COO}\cdot(\mathrm{ads}) \rightarrow \mathrm{CO}_2 + R \rightarrow \text{products}$$

A different, continuous deactivation of catalyst was found when no water vapor was present in the gas feed. This continuous loss of activity is reminiscent of the observation by Dibble and Raupp (*6*) that, for trichloroethylene photocatalyzed oxidation, a water-free feed led ultimately to a complete

loss of activity, whereas the presence of trace water allowed indefinite maintenance of activity. In the absence of feed water, their catalyst surface presumably became exhausted of the hydroxyls groups required for hole trapping and the formation of hydroxyl radicals that are responsible for organic oxidation. A potentially important difference is that water itself is a reactant for TCE destruction but is a product of photocatalyzed oxidation of less substituted hydrocarbons.

CONCLUSIONS

Trace (1–260 mg/m^3) concentrations of acetone, 1-butanol, butyraldehyde, formaldehyde, and *m*-xylene in air were successfully diminished by degradation (oxidation) in the presence of near-UV-illuminated TiO_2 anatase powder. Integral conversion rate data from single component runs provided kinetics parameters for a Langmuir–Hinshelwood rate expression. No reaction intermediates of acetone photooxidation were detected; we assume that acetone was eventually converted to CO_2. Butyraldehyde was the main product of 1-butanol photooxidation, but no 1-butene was detected. Formaldehyde photooxidation at levels of 6–90 ppm were carried out with no products detected via flame ionization.

Catalyst deactivation was noted only when photooxidizing 1-butanol or butyraldehyde. The activity was recovered by illuminating the TiO_2 photocatalyst in the presence of pure air, indicating the oxidizable nature of the deactivating species.

The ability of the catalyst to react an aldehyde, an alcohol, a ketone, and an aromatic at trace levels, along with prior literature demonstrating the conversion of simple alkanes, trichloroethylene (but see (*27*)), toluene, and several odor-associated compounds, indicates that all major classes of trace oxidizable air contaminants may be candidates for photocatalytic destruction.

The multiple roles of water in gas–solid photocatalysis deserve further exploration.

APPENDIX

The mass transfer influence is unimportant. Consider an illustrative run condition: Butanol feed rate = 11.3 μg/min; air feed rate = 0.0875 g/min; butanol feed concentration ($C_{i,B}$) = 1.611×10^{-7} g/cm^3; butanol reaction rate (J_i) = 2.78 μg/min = 4.63×10^{-8} g/s; superficial velocity = 22.3 cm/min; superficial flow cross section = 3.14 cm^2; superficial mass velocity (G) = 4.6×10^{-4} g/cm^2 · s; Reynolds number (Re) = $D_p \cdot G/\mu$ = 0.135; Schmidt number (Sc) = $\mu/\rho \cdot D$ = 0.136.

Packed bed j factor correlation (*10*):

$$\varepsilon_B j_D = \frac{1.09}{\mathrm{Re}^{2/3}}$$

with $\varepsilon_B = 0.4$, $j_D = 10.35$.

External mass transfer coefficient:

$$K_{c,i} = \frac{G}{\rho}\mathrm{Sc}^{-2/3} j_D = \frac{J_i}{C_{i,B} - C_{i,s}}.$$

Illuminated mass is 3.14 cm^2 · 4.5×10^{-4} cm · 3.8 g/cm^3 $\approx$ 5.4×10^{-3} g. A_c, the illuminated surface area, is 5.4×10^{-3} g · 5×10^5 cm^2/g = 2.68 cm^2

$$\frac{J_i}{A_c} = 1.72 \times 10^{-11} \frac{\mathrm{g}}{\mathrm{cm^2 s}}$$

$$C_{i,B} - C_{i,s} = \frac{J_i \rho}{G \cdot \mathrm{Sc}^{-2/3} j_D} = 1.19 \times 10^{-12} \frac{\mathrm{g}}{\mathrm{cm}^2}$$

$$C_{i,s} = 1.61 \times 10^{-7} \frac{\mathrm{g}}{\mathrm{cm}^3}$$

$$\frac{C_{i,B} - C_{i,s}}{C_{i,B}} = 7 \times 10^{-6} = 7 \times 10^{-4}\%.$$

Bulk and near-surface gas-phase concentrations of 1-butanol are virtually identical. No mass transfer influence is present, and data thus represent intrinsic chemical kinetics of surface reaction.

ACKNOWLEDGMENTS

This work was supported by NASA Research Grant NAG 2-684 (Reactor, chemicals and analysis) and by the Ministerio de Educación y Ciencia of Spain (Post-

Doctoral Fellowship for J. Peral). We acknowledge helpful comments from NASA's Advanced Life Support Technology Program, Office of Aeronautics, Exploration and Technology (Program Manager, Ms. Peggy L. Evanich; Technical Monitor, Dr. Edwin L. Force). A preliminary version of this paper was presented at the August 1991 AIChE meeting in Pittsburgh, Pennsylvania.

REFERENCES

1. Ollis, D. F., *Environ. Sci. Technol.* **19,** 480 (1985).
2. Ollis, D. F., Pelizzetti, E., and Serpone, N., in "Photocatalysis: Fundamentals and Applications" (N. Serpone and E. Pelizzetti, Eds.), pp. 604–637. Wiley, New York, 1989.
3. Ollis, D. F., Pelizzetti, E., and Serpone, N., *Environ. Sci. Technol.* **25,** 1523 (1991).
4. Courbon, H., Formenti, M., Juillet, F., Lisachenko, A. A., Martin, J., and Teichner, S. J., *Kinet. Catal.* **14,** 84 (1973).
5. Ibusuki, T., and Takeuchi, K., *Atmospher. Environ.* **20,** 1711 (1986).
6. Dibble, L. A., and Raupp, G. B., *Catal. Lett.* **4,** 345 (1990).
7. Blake, N. R., and Griffin, G. L., *J. Phys. Chem.* **92,** 5698 (1988).
8. Bickley, R. I., Munuera, G., and Stone, F. S., *J. Catal.* **31,** 389 (1973).
9. Suzuki, K., Satoh, S., and Yoshida, T., *Oenki Kagaku* **59,** 521 (1991).
10. "NIOSH Manual of Analytical Methods," 2nd ed., Vol. 7, Method P&CAM 354, DHHS (NIOSH) Pub. No. 82-100 (1981).
11. Hill, C. G., "An Introduction to Chemical Engineering Kinetics and Reactor Design," p. 475. Wiley, New York, 1977.
12. Egerton, T. A., and King, C. J., *J. Oil Col. Chem. Assoc.* **62,** 386 (1979).
13. Okamoto, K., Yamamoto, Y., Taneka, H., and Itaya, A., *Bull. Chem. Soc. Jpn.* **58,** 2023 (1985).
14. D'Oleivera, J., Al-Sayyed, G., and Pichat, P., *Environ. Sci. Technol.* **24,** 990 (1990).
15. Pruden, A. L., and Ollis, D. F., *J. Catal.* **82,** 404 (1983).
16. Boonstra, A. H., and Mutsaers, C. A. H. A., *J. Phys. Chem.* **79,** 1694 (1975).
17. Plog, B. A., Ed., "Fundamentals of Industrial Hygiene," p. 775. National Safety Council, 1988.
18. Pitchat, P., Herrmann, J., Courbon, H., Disdier, J., and Mozzanega, M., *Can. J. Chem. Eng.* **60,** 27 (1982).
19. Munuera, G., Rives-Arnau, V., and Saucedo, A., *J. Chem. Soc. Faraday Trans. 1* **75,** 736 (1979).
20. Bickley, R. I., and Stone, F. S., *J. Catal.* **31,** 389 (1973).
21. Primet, M., Pichat, P., Mathieu, J., *J. Phys. Chem.* **75,** 1216 (1971).
22. Primet, M., Pichat, P., Mathieu, J., *J. Phys. Chem.* **75,** 1221 (1971).
23. Cunningham, J., Hodnett, B. K., Ilyas, M., Tobin, J., and Leahy, E. L., *Faraday Discuss. Chem. Soc.* **72,** 283 (1981).
24. Djeghri, N., and Teichner, S. J., *J. Catal.* **62,** 99 (1980).
25. Formenti, M., Juillet, F., Meriadeau, P., and Teichner, S. J., *Chem. Technol.* **1,** 680 (1971).
26. Cunningham, J., and Hodnett, B. K., *J. Chem. Soc. Faraday Trans. 1* **77,** 2777 (1981).
27. In a letter dated 5/11/92, Tom Milne of NREL, Golden, Colorado notified us that he and Mark Nimlos have detected "phosgene concentrations up to about 75 ppmv... at 98% TCE destruction (chlorine concentrations were comparable). This is well above the threshold limit value of 0.1 ppmv."